

RESEARCH

Open Access



# Slab Reinforcement Contributions to Negative Moment Strength of Reinforced Concrete T-Beam with High Strength Steel at Exterior Beam-Column Joints

Zhamilya Mamesh<sup>1</sup>, Dilnura Sailauova<sup>1</sup>, Dichuan Zhang<sup>1\*</sup> , Hyunjin Ju<sup>2</sup>, Deuckhang Lee<sup>3</sup> and Jong Kim<sup>1</sup>

## Abstract

Previous studies have revealed that the contribution of slab reinforcement to the T-beam flexural strength in negative moment regions are not negligible for the seismic capacity design. An effective slab width (i.e., effective width of flanged section) has been proposed, within which the slab reinforcement needs to be included in the calculation of the beam nominal flexural strength in negative moment regions. These studies mainly focused on the cases using normal-strength steel in moment resisting frames. However, recently high-strength steel has been widely used in reinforced concrete moment resisting frames in high seismic regions to avoid congestion near beam-column joints. The use of high-strength steel may affect the beam stiffness due to the fact that it will require less amount of reinforcement, and result in a different normal stress distribution compared to the case with normal-strength steel. Therefore, this paper investigates the slab reinforcement contribution to the flexural strength of the reinforced concrete T-beam designed with high-strength steel in negative moment regions at exterior beam-column joints, for which nonlinear pushover analyses were conducted. Beam reinforcement grade was considered as a primary parameter with several other design variables including slab thickness, height, and span length of the beam. Analytical results show that the use of high-strength steel can result in a wider effective slab width than the case of normal-strength steel for calculating the beam nominal flexural strength under the negative moment. Based on these results, new design equations were proposed.

**Keywords** Effective slab width, High strength steel, Negative moment strength, Seismic design, Nonlinear finite element analysis

Journal information: ISSN 1976-0485 / eISSN 2234-1315.

\*Correspondence:

Dichuan Zhang  
dichuan.zhang@nu.edu.kz

<sup>1</sup> School of Engineering and Digital Sciences, Nazarbayev University, 53 Kabanbay Batyr Ave, Astana, Republic of Kazakhstan 010000

<sup>2</sup> Hankyong National University, 327, Jungang-Ro, Anseong-Si 17579, Gyeonggi-Do, Korea

<sup>3</sup> Chungbuk National University, 1 Chungdae-Ro, Seowon-Gu, Cheongju 28644, Chungbuk, Korea

## 1 Introduction

In high seismic regions, reinforced concrete (RC) moment resisting frames might have a congestion issue due to excessive amounts of reinforcement in beam-column joints. Moreover, this congestion may result in high cost and low efficiency during construction (Kotsovos et al., 2013; Madias et al., 2017). One of the effective solutions to resolve this issue can be the use of high-strength steel (HSS) instead of normal-strength steel, particularly in beam-column joints of the moment-resisting frame to satisfy high seismic detailing requirements (NIST, 2014; Shahrooz et al., 2011). For the same structural

component, application of HSS can significantly reduce the required amount of steel in comparison to normal-strength steel, thus preventing the reinforcement congestion and decreasing the material cost (Alavi-Dehkordi et al., 2019; Alaei & Li, 2017). Recently, ACI 318 (2019) has allowed using HSS in special moment frames, but with limited yield strength up to 550 MPa due to the serviceability issue. Despite the restrictions, several researchers have used HSS with the yield strength higher than 550 MPa in beam-column joints, thus showing that the crack width was within the allowable limits in structures with HSS (Alaei & Li, 2017; Alavi-Dehkordi et al., 2019; Chang et al., 2014).

The lateral-load resisting components (beams, columns, and beam-column joints) are the most critical elements in the structural design for the reinforced concrete moment resisting frame (Wang et al., 2016). Current seismic design practices in Europe, North America, and Asian regions have commonly adopted a so-called “strong-column and weak-beam” concept to allow the yielding of beams under earthquakes. According to this criterion, the flexural strength of columns must be at least 20% greater than the actual flexural strength of the beams at the joint (ACI 318, 2019; Eurocode 8, 1996). Therefore, it is important to accurately estimate the flexural strength of the beam during the seismic design. The slab reinforcement contribution is not significant for the positive moment since the slab is under compression. However, for the negative moment, when the top of the beam is under tension, some portions of the slab reinforcement located close to the beam contribute to the moment resistance, and this contribution becomes less depending on the distance from the center of the beam due to the shear lag effect. Existing studies have proposed an effective slab width, in which slab reinforcement would contribute to the flexural strength of the beam (Durrani & Zerbe, 1987; Pantazopoulou et al., 1988; Qi et al., 2010; Zhen et al., 2009). However, the equations for the effective slab width in the tension zone suggested in the existing studies as well as those specified in code provisions are primarily for the structures configured with normal-strength steel. Since the use of HSS may affect the normal stress distribution in the beam and slab reinforcement, it is important to identify whether the effective slab width for the beams with normal-strength steel is applicable to the beams with HSS. However, only few studies have been conducted regarding the slab reinforcement contribution and effective slab width of the beam with HSS in the tension zone.

For a better understanding of this phenomenon, this paper investigates the effect of beam reinforcement strength on the effective slab width for the exterior beam-column joints through analytical studies.

Nonlinear static pushover analyses were conducted. To this end, a three-dimensional (3D) multi-truss model was adopted by applying the vertical displacement at the beam free end for an idealized beam-column-slab assembly. The beam reinforcement strength was set as the key influential factor, while several other parameters affecting the effective slab width were also considered in the study including slab thickness, height, and span length of the beam.

## 2 Background

### 2.1 Effective Slab Width

In the negative moment region, the imbalance of tension forces between mid-span and end support induces the shear flow at the web-flange joint, as shown in Fig. 1. This shear flow makes the normal stresses in the flange lag behind that of the web, thus causing *Shear lag*. Due to the uneven stress distribution, the concept of *effective slab width* has been introduced to simplify the beam section analysis (Moffatt & Dowling, 1978). The effective slab width ( $B_{eff}$ ) represents reduced slab width with a uniform stress distribution that replaces the actual stress distribution to be equivalent to the total force.

In seismic design, the “strong-column and weak-beam” principal has been implemented to make structural beams with high ductility weaker than columns with low ductility, so that the structure could have a ductile response rather than brittle collapses. According to Section Clause 18.7.3.2 in ACI 318-19, at a beam-column joint, it is required that the total moment capacity of the column should be 1.2 times greater than that of the beam to ensure “strong-column and weak-beam” design:

$$\sum M_{nc} \geq 1.2 \sum M_{nb}, \quad (1)$$

where  $\sum M_{nc}$  = the sum of the nominal moment capacities of columns at the surface of the joint;  $\sum M_{nb}$  = the sum of the nominal moment capacities of beams at the surface of the joint. Under negative moment, slab tension reinforcement lying within the effective width ( $B_{eff}$ ) would contribute to nominal beam flexural strength,  $M_{nb}$ .

A number of studies have suggested design equations for the effective slab width to evaluate the contribution of slab reinforcement to the beam flexural strength (Durrani & Zerbe, 1987; Ning et al., 2016; Pantazopoulou, 1988; Qi et al., 2010; Zhen et al., 2009). Table 1 summarizes the suggested design equations in the existing studies and building codes with key parameters used in the equations. The parameters include beam height, slab thickness, and span length of beam. Moreover, all the equations are suggested for RC beams reinforced with normal-strength steel, which requires further studies on

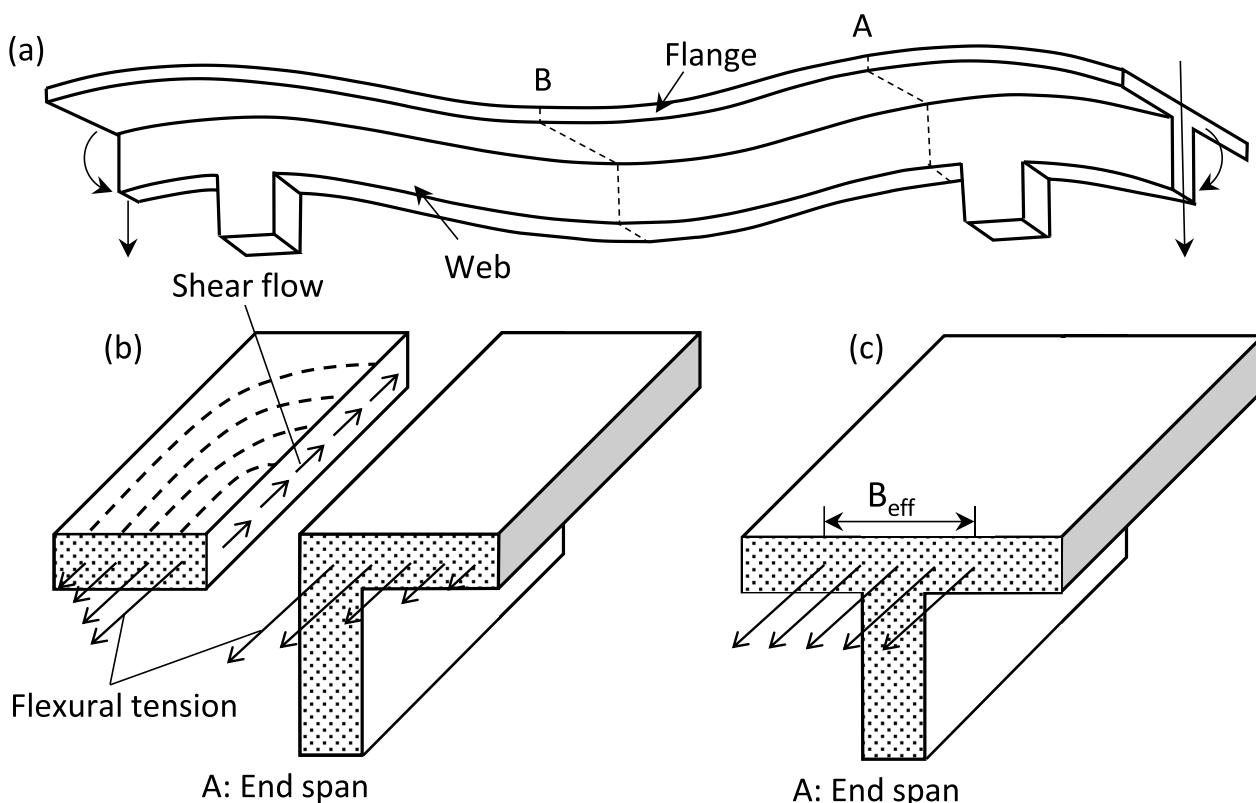


**Fig. 1** Shear flow occurred in the flange of the T beam under a negative moment: **a** Beam span; **b** Actual; **c** Assumed uniform stress distribution for design

**Table 1** Effective slab width in code provisions and existing studies

Codes/existing studies	Equations for $B_{eff}$	Parameters	Beam reinforcement
ACI 318 (2019)	$b + \text{Min}(16t_s, L_0, L_n/4)$	$b, t_s, L_0, L_n$	Normal-strength steel
Eurocode 8 (1996)	$b + 4t_s$	$b, t_s$	
SNiP code (1997)	$\text{Min}(L/6, b + 12t_s)$	$b, t_s, L$	
Durrani and Zerbe (1987)	$b + 2h$	$b, h$	
Pantazopoulou et al. (1988)	$b + 6d$	$b, d$	
Zhen et al. (2009)	$b + 4h$	$b, h$	
Qi et al. (2010)	$b + \text{Min}(\text{Max}(L/5, 3h), L_0/2)$	$b, h, L, L_0$	
Ning et al. (2016)	$b + 5.4h$	$b, h$	

$b$  = web thickness,  $t_s$  = slab thickness,  $h$  = beam height,  $d$  = beam effective depth,  $L_0$  = clear distance to the adjacent web,  $L_n$  = clear span,  $L$  = beam span

the effective slab width for RC beams configured with HSS.

**2.2 Review of RC Structures with High-Strength Steel**

The use of HSS reinforcement can be an effective method in reducing the required amount of steel in RC members, thus resulting in cost savings in material, transportation, and placement (Alavi-Dehkordi et al., 2019; Shahrooz et al., 2011). Different types of HSS have been developed,

and those are currently available in international markets (NIST, 2014).

Various grades of reinforcing steel have been adopted in ASTM specifications based on their production methods. ASTM A706 includes deformed and plain low alloy steel reinforcing bars with limited mechanical properties (ASTM, 2016a). Their Grade 60 and 80 reinforcements were the first HSS bars used for seismic purposes in moment-resisting frames and special structural walls

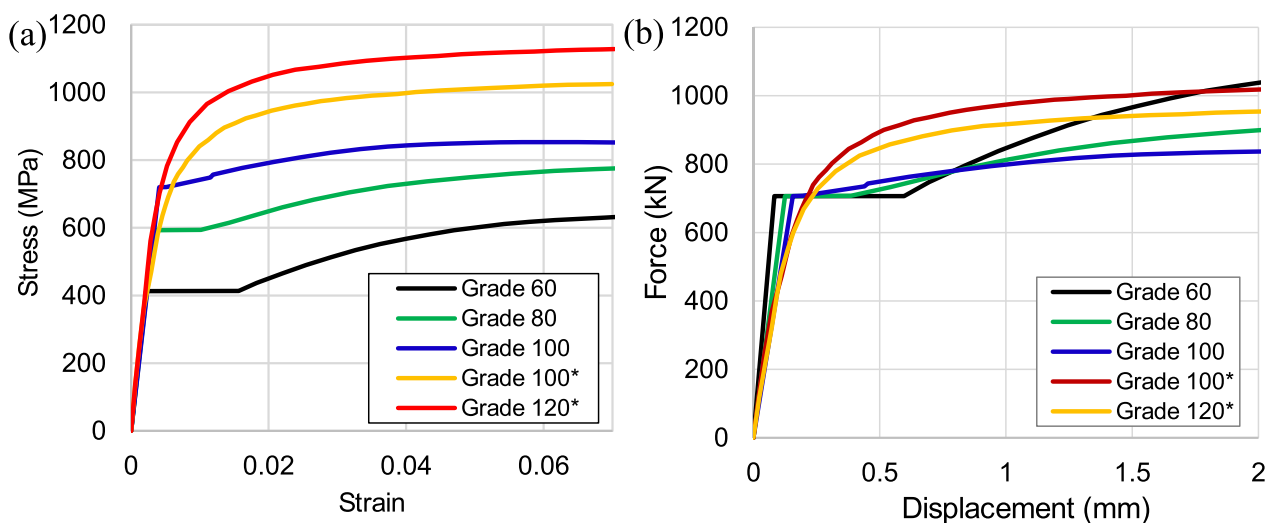


**Fig. 2** a Stress–strain curves; b force–displacement curves of different reinforcement grades (\*without clear yielding points)

(NIST, 2014). ASTM A615 presents the deformed and plain carbon steel bars which include HSS up to Grade 100 (ASTM, 2016b). ASTM A1035 reinforcing steel produced in Grades 100 and 120 is composed of chromium alloy with low carbon content (NIST, 2014). Fig. 2a presents the typical stress–strain curves for different grades of HSS from various studies (Barbosa et al., 2016; CRSI, 2016; El-Hacha & Rizkalla, 2002; Huq, 2018). As can be seen, both A706 and A615 have clearly defined yielding points (from Grade 60–100), while ASTM A1035 reinforcing steel shows no clear yielding point (from Grade 100–120). Fig. 2b converts the stress–strain curves into the force–displacement curves by imposing the same yield force and gauge length for different steel grades. Since the yield strength for different steel grades is different, the cross-section area does also vary. As seen in Fig. 2b, the high-strength steel shows a lower stiffness than the normal-strength steel.

There have been numerous studies on the seismic behavior of HSS in RC structures including structural walls, beams, columns, and beam-column joints (Alaee and Li, 2017; Alavi-Dehkordi et al., 2019; Cheng et al.,

2016; Li et al., 2018). Also, some studies were reported on the beam-column joints in both interior and exterior cases (Alaee and Li, 2017; Alavi-Dehkordi et al., 2019; Chang et al., 2014). The yield strength of reinforcement in these studies ranged from 420 to 1034 MPa. Additionally, It has been discovered that the use of HSS as a beam longitudinal reinforcement with decreased cross-sectional area resulted in the reduction of energy dissipation capacity and stiffness of beam-column joints. Besides, beam-column assemblies configured with a lower reinforcement ratio of HSS can obtain a comparable load-carrying capacity to those with normal-strength steel (Alaee & Li, 2017; Alavi-Dehkordi et al., 2019). Aoyama (2001) studied slab effect on flexural behavior of beams using HSS for slab reinforcement. The assembly consisted of beam and slab with 689 MPa and 1034 MPa for beam and slab reinforcements, respectively. It has been observed that high-strength slab reinforcement contributes to the beam flexural strength in the negative moment regions (Aoyama, 2001). However, his study did not evaluate the effective width of the slab for the beam with HSS.

**Table 2** Study parameters

Beam reinforcement			Type	Slab thickness, $t_s$ (mm)	Beam height/Beam span, $h/L$ (mm/mm)
Grade	Yield strength (MPa)	Reinforcement ratio, $\rho$ (%)			
60	420	1.5	Type I (with a clear yielding point)	100	500/5000
80	593	1		150	600/6000
100	690	0.85	Type II (without a clear yielding point)	200	700/7000
120	830	0.7			

### 3 Description of Analytical Study

#### 3.1 Study Parameters

Several parameters were considered in this study to investigate their effects on the normal stress distribution and the slab effective width, as presented in Table 2. The main study parameter is the beam reinforcement grade, i.e., the yield strength, which ranged from 420 to 830 MPa. To keep a similar strength for the beam, the total yielding force ( $T = f_y A_s$ ) was set to be constant for the beam with different steel grades, which subsequently resulted in different beam reinforcement ratios ( $\rho$ ). Also, two types of beam reinforcement grades (Type I and Type II) were used in this study. Grades 60, 80, and 100, which have a clear yielding point, are applied to Type I, while Grades 100 and 120 without a clear yielding point are considered as Type II reinforcement.

Other parameters considered in this study are slab thickness ( $t$ ), height ( $h$ ), and span length of beam ( $L$ ) because most of the studies included these parameters in their design equations for the effective slab width. Typically, the height of beam varies with the span length. Therefore, in this study, those parameters were chosen to be varied proportional, as summarized in Table 2.

The other study parameters were kept as constants to represent typical dimensions of beam-column-slab assemblage at an exterior joint. Dimensions of transverse beams are taken the same as that of the longitudinal beam under study. The beam width is set as 50% of the beam height. The square column with a length of 3 m and the same height as the beam height was used. The slab reinforcement is kept as Grade 60 and #3 rebar with a cross-sectional area of 71 mm<sup>2</sup> with a constant spacing of 150 mm. Compressive and tensile strength of unconfined concrete are 41 MPa and 4 MPa, respectively.

#### 3.2 Model Development

The 3D multi-truss modeling approach was adopted to construct an exterior beam-column-slab assemblage, rather than a 3D model with solid elements. The multi-truss model has less numbers of degree of freedoms as compared to the solid model, which is able to save the computational cost. The solid model approximates the discrete cracking behavior with continuous plasticity. It tends to have a concentrated deformation in the cracking region which causes deformation incompatibility along the height of the beam and the width of the slab. On the other hand, the multi-truss model is able to capture the discrete cracking behavior through the deterioration of individual nonlinear truss element and the elastic beam element inside the truss assemblage is able to maintain the deformation compatibility in the cracking zone. The 3D multi-truss modeling approach was used to model reinforced concrete shear walls under seismic loading and showed good agreement with the test

results (Panagiotou et al. 2012). This approach has also used in the modeling of precast concrete connectors (Zhang et al., 2016), and the models were verified by structural tests (Zhang et al., 2011).

The analytical model has been developed by using the commercial finite-element (FE) analysis platform ABAQUS, as shown in Fig. 3. The model consists of two types of the elements considering the characteristics of components: (1) linearly elastic beam elements, which were used to model the transverse beam, column, and vertical elements of beam and slab; (2) nonlinear truss elements for the concrete beam and slab as well as the longitudinal reinforcement as shown in Fig. 3. The assemblage represents a cut of the exterior joint from inflection points in the moment resisting frame. The slab is modeled with a layer of horizontal nonlinear trusses placed at the center of the slab thickness. The longitudinal beam is modeled with a layer of vertical nonlinear trusses placed at the center of the beam width. These layers of trusses were divided into 40 mm by 40 mm subsets to represent the solid concrete. The subset consists of horizontal trusses, diagonal trusses, and elastic beams. Beam and slab reinforcement are modeled as nonlinear truss elements and embedded in the truss layers. The transverse beam and column are modeled as 3D elastic beam elements and are rigidly connected to the slab nodes and beam nodes, respectively. Pinned boundary conditions (i.e.,  $U_X = U_Y = U_Z = 0$ , where  $U$  denotes the translation, and  $X$ ,  $Y$ , and  $Z$  indicate each direction in three dimensional space) were applied at the top and bottom nodes of the column. Beam nodes were constrained in the  $Z$ -axis direction ( $U_Z = 0$ ) to prevent out-of-plane movement. The length of each beam and truss element is set to be 40 mm based on a preliminary mesh sensitivity study (Mamesh, 2022). Nonlinear pushover analyses were conducted by applying an incremental downward vertical displacement ( $\Delta$ ) at the beam end nodes.

The concrete material is simulated with the concrete damaged plasticity model (CDP), which is implemented in ABAQUS software (2010) with isotropic damage. The concrete model is able to capture brittle tensile cracking and compressive crushing behavior. Fig. 4a, b present the compressive and tensile stress–strain relationship of the confined and unconfined concrete based on material properties obtained from tests conducted by Durrani and Zerbe's (1987), respectively. The confined concrete behavior was simulated by using Mander's model (1988), and it was applied to the inner horizontal trusses of the beam, as shown in Fig. 4c.

The concrete was modeled as multi-truss elements to achieve an equivalent strength and stiffness for a solid concrete block. As shown in Fig. 5, solid elements were converted into the subset of truss elements, where its size is 40 mm ( $b_e = L_e$ ), by matching their global strength and stiffness for tensile, compressive, and shear behaviors.

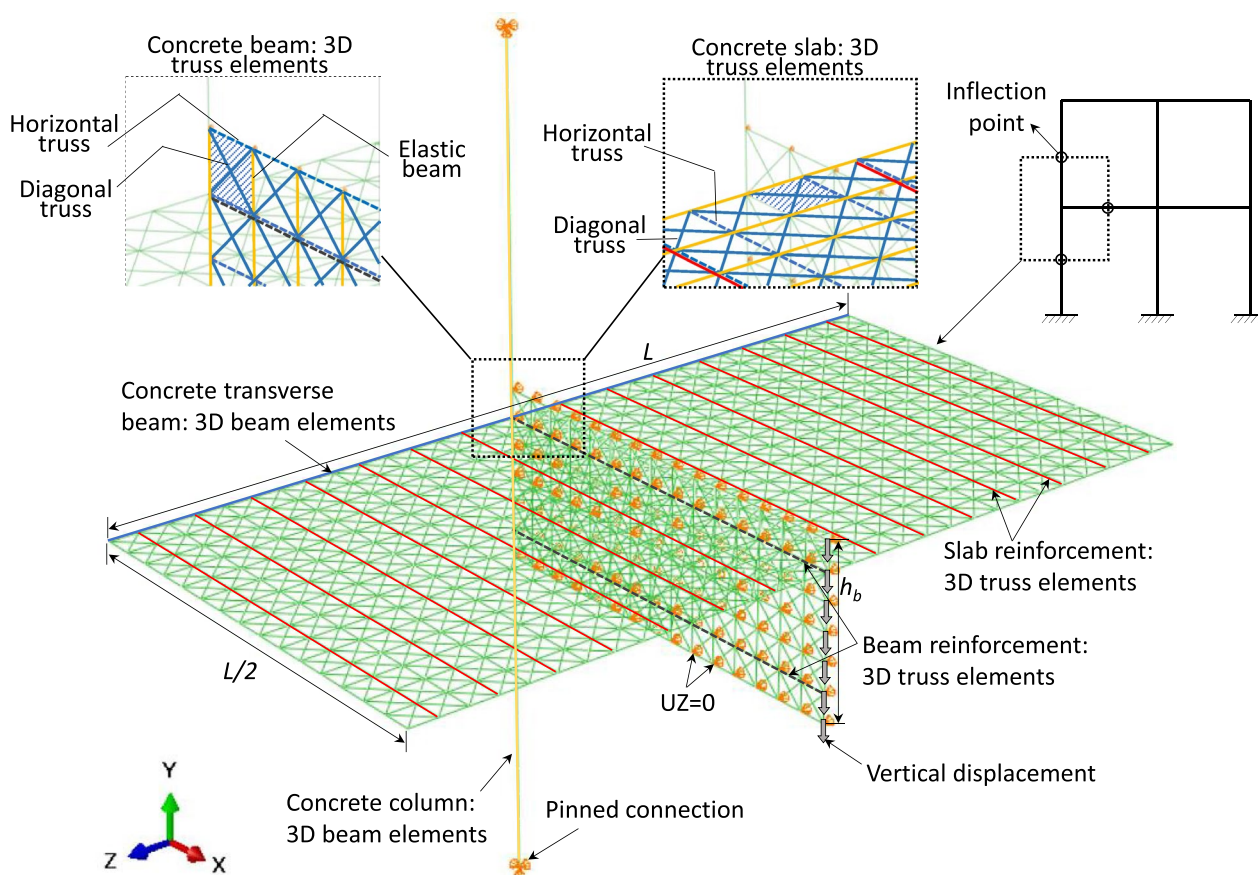


**Fig. 3** Multi-truss model of beam-column-slab assemblage

Horizontal trusses were used to model the tension and compression behavior of concrete, while diagonal trusses ( $\theta = 45^\circ$ ) were used to model the coupled shear and axial behavior of concrete. Elastic vertical beams were used to keep deformation compatibility after the truss element cracks or crushes. By assigning concrete strength (i.e., tension and compression) to the truss element, the cross-sectional area and Young’s modulus of each truss element were calibrated to achieve the same global strength and stiffness as the solid concrete. The calculated values for beams and slabs are presented in Table 3, and the detailed calculation and calibration process for the multi-truss element can be found in elsewhere (Mamesh, 2022).

For the longitudinal reinforcement, the same mechanical properties of reinforcing bar shown in Fig. 3 were directly assigned to the truss element. The bonding between reinforcement and concrete was assumed to be rigid (i.e., no bond slip condition).

### 3.3 Model Validation

An experimental study conducted by Durrani and Zerbe (1987) was used to validate the analytical model. The

study investigates the exterior beam-column-slab assemblage subjected to cyclic loadings. The column has a square section with a height of 305 mm. The longitudinal beam with a section of  $381 \times 254$  mm has a length of 1.676 m. The slab thickness and width are 102 mm and 1778 mm, respectively. A transverse beam with a section of  $381 \times 254$  mm was provided. The dimensions of the assemblage and reinforcement detailing are given in Fig. 6. The longitudinal beam and column ends were provided with hinged connections. Concrete strength on the day of the test was 40.68 MPa, and the specimen was configured with Grade 60 reinforcement. During the test, cyclic vertical displacements were applied at the end of the longitudinal beam. One cycle per amplitude was executed with an increasing amplitude of 12.7 mm. The maximum amplitude is 101.6 mm at the 8th cycle, which is corresponding to a 6% inter-story drift. The beam and slab reinforcement were instrumented with strain gauges to measure the strain/stress at the maximum displacement of each loading amplitude. More information for the tests can be found in Durrani and Zerbe (1987).

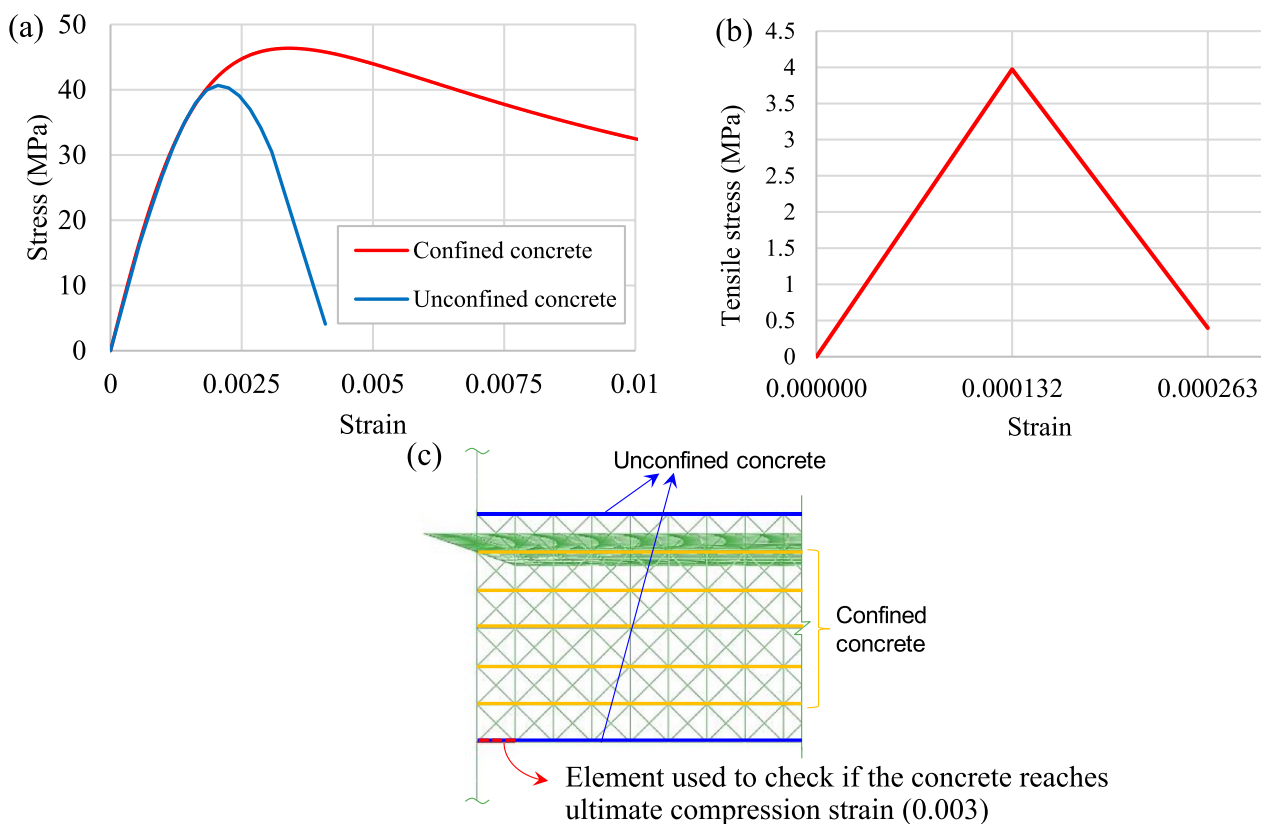


**Fig. 4** Modeling of concrete: **a** compression behavior, **b** tension behavior, and **c** truss model

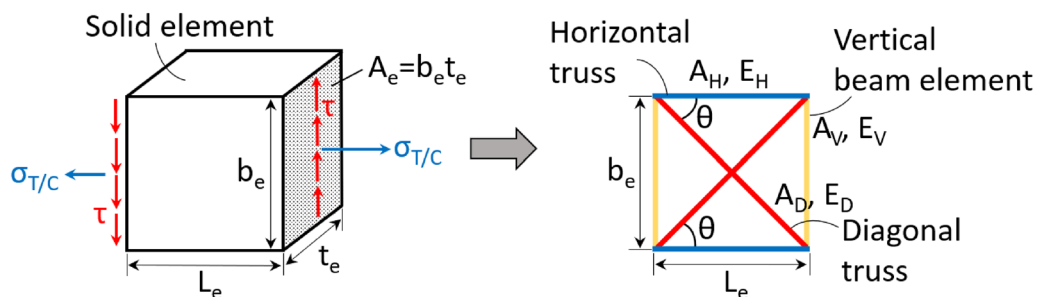


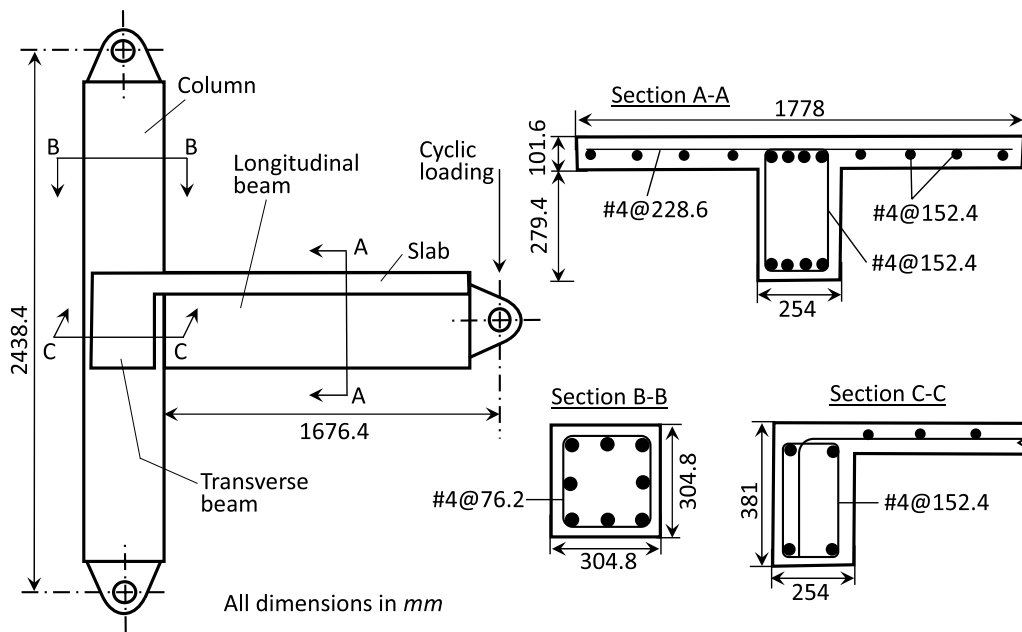
**Fig. 5** Conversion from solid to truss elements

**Table 3** Input parameters of truss elements for concrete model

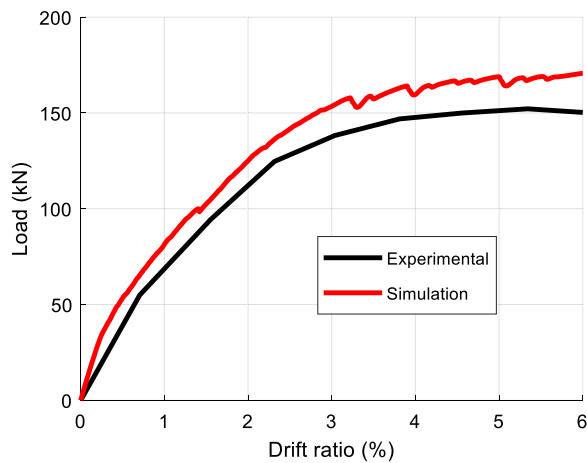
Elements	Beam		Slab	
	Horizontal truss	Diagonal truss	Horizontal truss	Diagonal truss
Cross-sectional area (mm <sup>2</sup> )	3923	1298	1800	196
Young's modulus (GPa)	29.5	132.55	25.72	355.01

Fig. 7 shows the load (reaction at the beam free end) vs. drift ratio (vertical displacement normalized by the length of the beam) response of the multi-truss model

in comparison with the experimental data. The multi-truss model shows similar behavior as observed from the experiment. The discrepancy in overall behavior might be



**Fig. 6** Reinforcement detailing and dimensions of the experimental set-up, modified from (Durrani & Zerbe, 1987)



**Fig. 7** Load vs. drift ratio curves of simulation and experiment

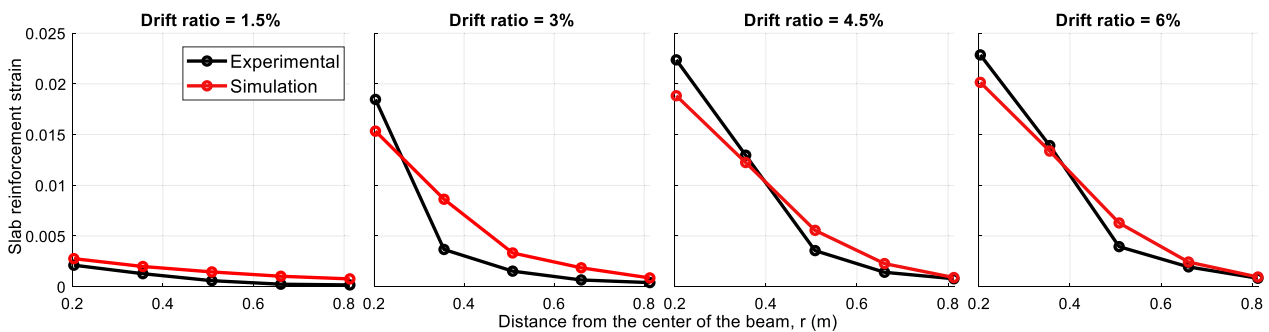
attributed to the fact that a cyclic loading was applied in the test while a monotonic pushover was applied in the model.

Fig. 8 demonstrates the strain distribution in slab reinforcement for the multi-truss model compared to experimental results at different drift ratios. The simulation reasonably captures the general trend of experimental results.

## 4 Analytical Results

### 4.1 Effects of Beam Reinforcement Grade

This section aims to evaluate the effects of beam reinforcement grade on the slab reinforcement contribution to the beam flexural strength for the cases with  $t_s=150$  mm,  $h=500$  mm, and  $L=5000$  mm, where  $t_s$



**Fig. 8** Strain distribution in slab reinforcement at different drift ratios

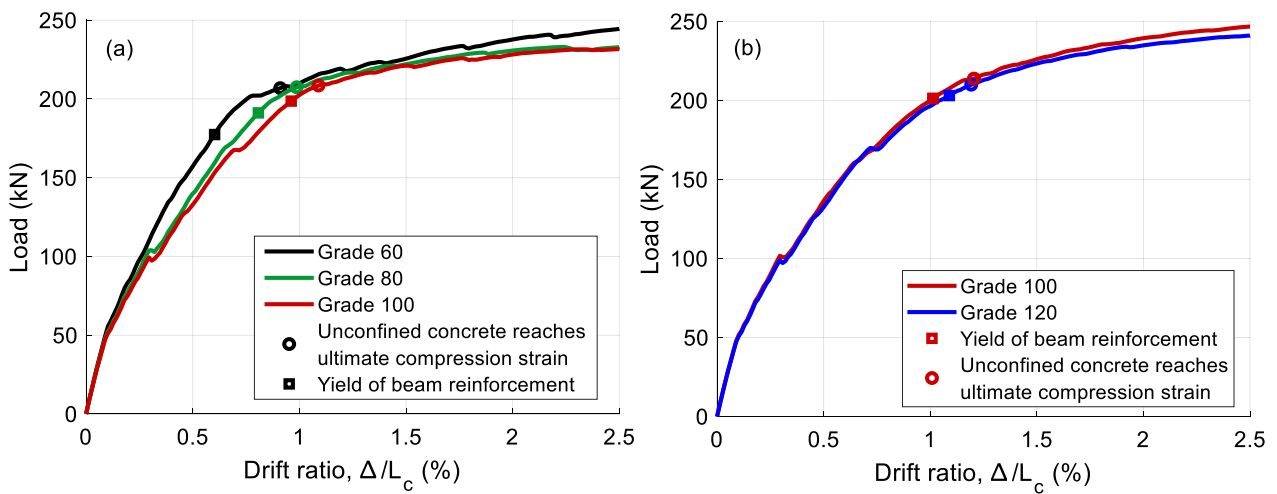


**Fig. 9** Load vs. drift ratio response for the model with (a) Type I and (b) Type II beam reinforcement

is the slab thickness,  $h$  is the beam height, and  $L$  is the length of a beam member.

Fig. 9a, b shows the load vs. drift ratio curves for the model with Type I and Type II condition of the beam reinforcement grades, respectively. It highlights the points at the key events, such as yielding of beam reinforcement and the unconfined concrete strain reaches the ultimate strain,  $\epsilon_{cu} = 0.003$ . The load-drift ratio responses indicate that the strength of the assemblage can still increase after the unconfined concrete strain reaches the ultimate strain due to the fact that the confined concrete can still carry the compression force. The

load-drift ratio responses are similar for all cases due to the beam was designed with the same strength regardless of the grade of the steel; however, the beam with a higher steel grade shows a lower initial stiffness and delayed reaching of ultimate strain at a larger drift ratio. This is because the HSS reinforcement has a smaller total cross-sectional area than the normal-strength steel does for achieving a similar total tensile strength. Although the beam flexural stiffness is not significantly affected by the steel grade (see Fig. 9a), this small influence can play a role in changing the stress distribution of the slab reinforcement which can be observed in Fig. 10.

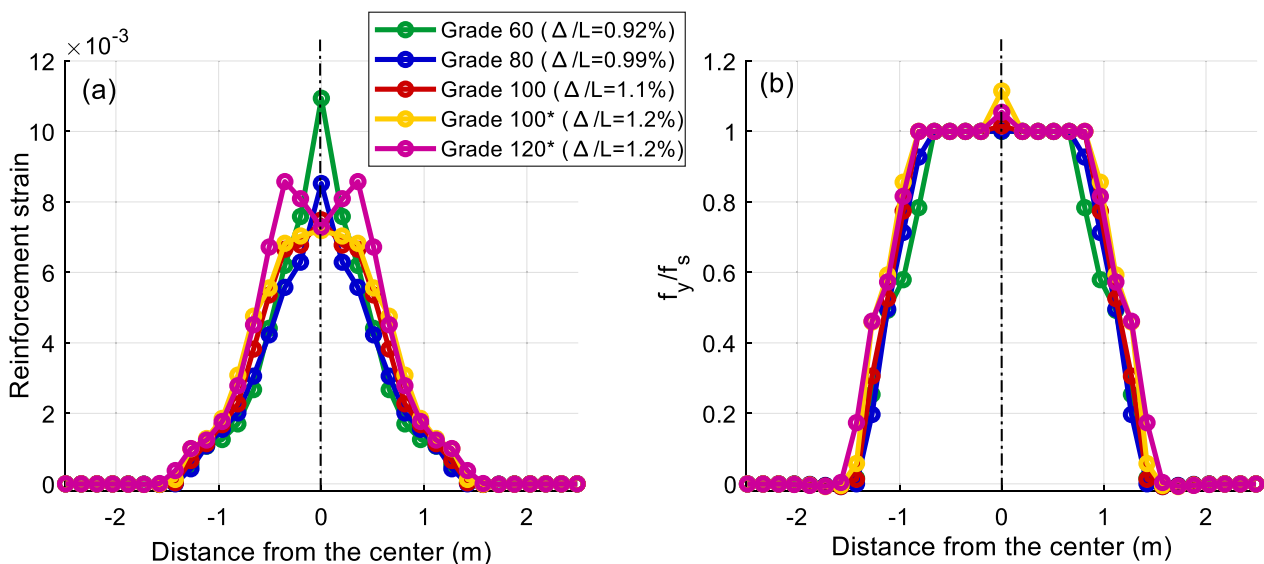


**Fig. 10** Stress and strain distribution in the reinforcement along the slab when the unconfined concrete reaches ultimate compression strain: a Strain and (b) Normalized stress (\*Type II reinforcement)

Fig. 10a, b shows distributions of strain and corresponding normalized stress (by the yield stress) in reinforcement along the width of the slab, respectively, at the point when unconfined concrete reaches ultimate compression strain. As shown in Fig. 10, the strain and stress in the slab reinforcement gradually reduce as a considered location moves from the center of the beam to the edge of slab due to the shear lag effect. The unconfined concrete reaching its ultimate compression strain occurs at larger drifts for HSS cases due to their higher flexibility as shown in Fig. 9. Therefore, the cases with HSS have a higher strain at the same location in the slab reinforcement, as compared to the case with normal-strength steel. As a consequence, when the beam reinforcement grade increases, the stress in the slab reinforcement increases and more slab reinforcements can be yielded. This trend indicates a wider effective width for the cases with HSS at the point when the unconfined concrete reaches its ultimate compression strain.

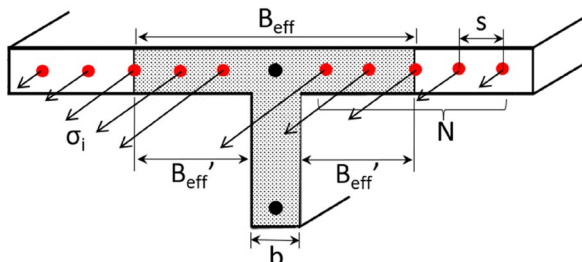


**Fig. 11** Calculation of effective slab width in negative moment regions

The contribution of the slab reinforcement to the beam flexural strength can be estimated by the summation of the tensile forces in the slab reinforcement at each side of the beam. The effective width ( $B_{eff}$ ) can then be calculated to have an equivalent total tensile force when the reinforcement within this width is considered to be yielded, as shown in Fig. 11.

The amount of slab reinforcement within the effective slab width can be determined by dividing the total tension force ( $F_n$ , summation of the tensile forces in all slab reinforcement) by the yield tensile force in a single slab rebar ( $A_b f_y$ ), which gives the number of slab reinforcement ( $N$ ) yielded in an average sense, as follows:

$$N = \frac{F_n}{A_b f_y} = \frac{A_b \sum \sigma_i}{A_b f_y} = \frac{\sum \sigma_i}{f_y}, \tag{2}$$

where  $A_b$  and  $f_y$  are the cross-sectional area and yield strength of single slab rebar, respectively, and  $\sigma_i$  is the actual stress in each slab reinforcement within one side overhanging as the stress/strain distribution is symmetric on both sides. The number of bars ( $N$ ) is then multiplied by slab reinforcement spacing ( $s$ ) to find overhanging effective width ( $B_{eff}'$ ), as follows:

$$B_{eff}' = N \times s. \tag{3}$$

On this basis, the effective slab width ( $B_{eff}$ ) can be computed by adding the beam width ( $b$ ) to the twice of the overhanging width, as follows:

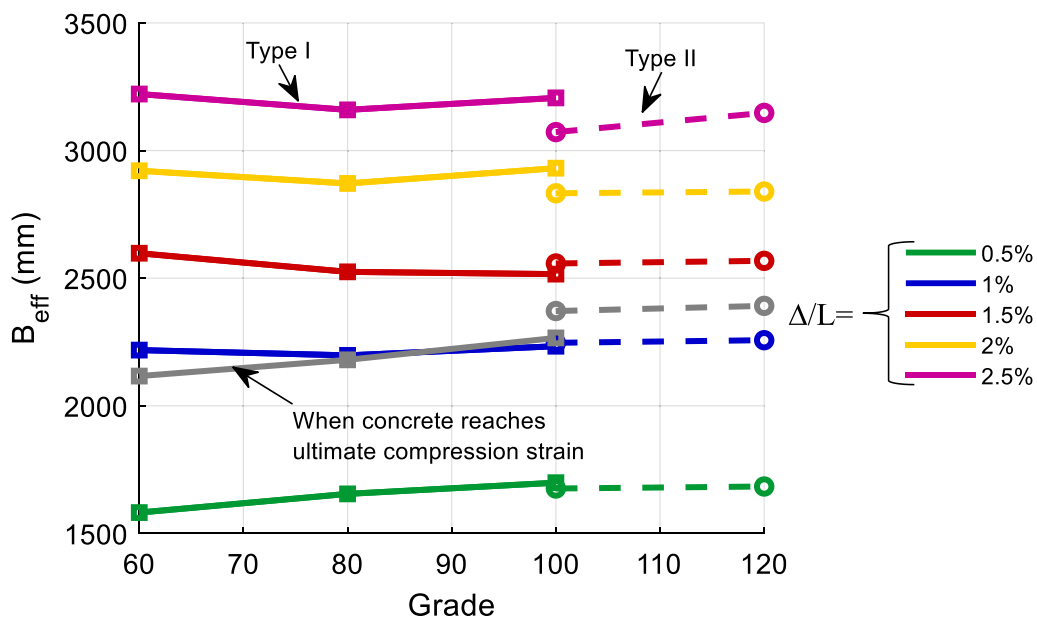


**Fig. 12** Effective slab width at different drift ratios

$$B_{eff} = b + 2B_{eff}' = b + 2 \frac{\sum \sigma_i}{f_y} s. \tag{4}$$

Fig. 12 shows the effective slab width calculated for the cases with different beam reinforcement grades using Eq. (4) at different drift ratios and the point when concrete reaches ultimate compression strain. It can be observed that the effective slab width increases as the drift ratio increases due to the stress/strain penetration into the slab. At large drift ratios from 1.5% to 2.5%, the effective slab width is similar regardless of the grades of the beam reinforcement. However, at lower drift ratios (<1%), the effective slab width increases with the increase of the beam reinforcement grade, particularly at a point when the unconfined concrete reaches ultimate compression strain. Since the nominal moment strength is typically defined at a point when the concrete reaches the ultimate compression stain, the effective slab width calculated for this point will be presented and discussed in the following sections.

#### 4.2 Effect of Slab Thickness

In this section, various slab thicknesses are chosen from 100 to 200 mm to evaluate its effect on the effective slab width calculated for the point when the unconfined concrete reaches ultimate compression strain. This point was also used for calculation of the nominal flexural strength according to ACI 318 (2019). Different beam reinforcement grades were also used, namely Grade 60 and Grade 80 for Type I, and Grade 120 for Type II. The height and span length of the beam member were kept as 500 mm and 5000 mm, respectively.

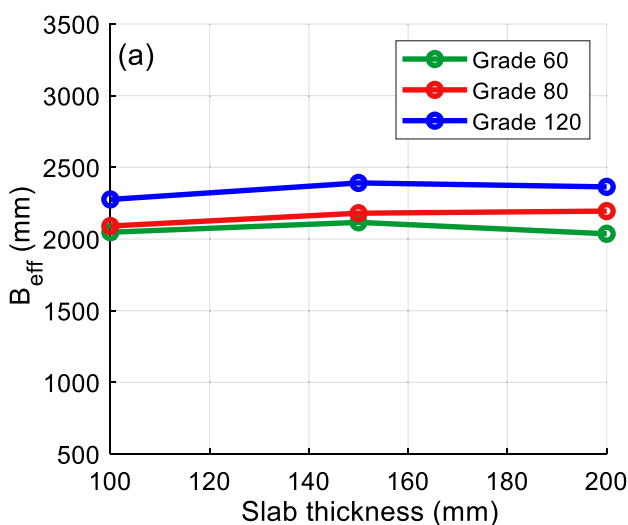


Fig. 13 shows the effect of the slab thickness on the effective slab width for the cases with different beam reinforcement grades. Increase in slab thickness showed no significant effect on  $B_{eff}$ . This is because the  $B_{eff}$  is calculated at the tension side, where the concrete has cracked, and its influence is limited. From Fig. 13a, it can be also confirmed that the  $B_{eff}$  increases with increase of the beam reinforcement grade. This increasing trend is similar among the different slab thicknesses, as observed in Fig. 13b, where the  $B_{eff}$  was normalized by the case with Grade 60 beam reinforcement. Therefore, the effect of slab thickness can be ignored for calculating effective slab width with HSS.

#### 4.3 Effect of Height and Span Length of Beam

In this section, the dimensional properties (i.e., height and span length) of the beam varied from 500 to 700 mm and 5000 to 7000 mm for the height and span length, respectively, to examine their effects on the effective slab width calculated for the point when the unconfined concrete reaches ultimate compression strain. Note that the ratio between the beam height and span length was set to be the same, and cases with different beam reinforcement grades were also considered. In addition, the slab thickness was kept as 150 mm.

Fig. 14 shows the effect of the height and span length of the beam on the effective slab width for the cases with different beam reinforcement grades. As shown in Fig. 14a, the higher the height/span length of the beam is, the slightly higher  $B_{eff}$  is. This trend is consistent with the studies in the literature (refer to Table 1). Fig. 14a also confirms that the  $B_{eff}$  increases with the increase of the beam reinforcement grade. This increase trend is almost

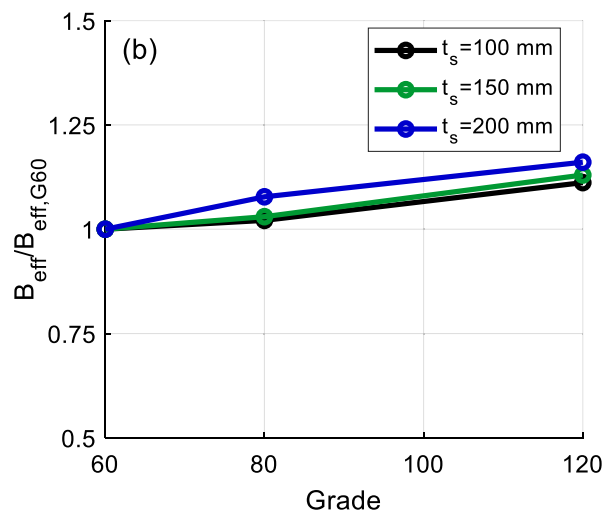
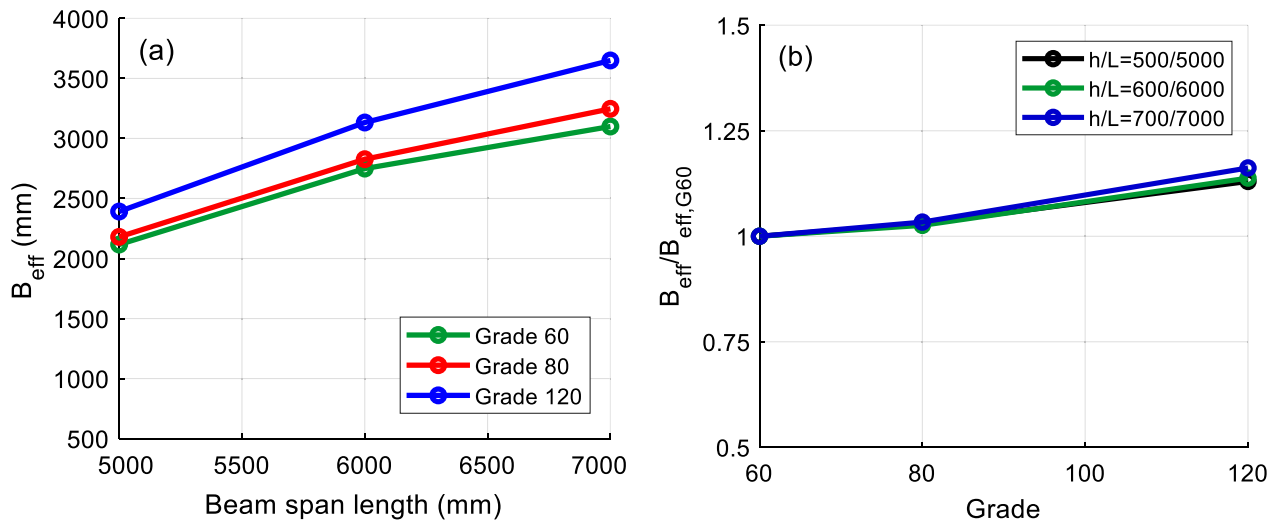


Fig. 13 Effect of the slab thickness on  $B_{eff}$ : a Absolute values and b Normalized values



**Fig. 14** Effect of the height/span length of the beam on  $B_{eff}$ : **(a)** Absolute values and **(b)** Normalized values

the same among the different heights/span lengths of the beam as observed in Fig. 14b, where the  $B_{eff}$  was normalized by the case with Grade 60 beam reinforcement. Therefore, the effect of the height/span length of the beam on the slab effective width can be considered independently.

### 5 Design Recommendations

The effective slab width calculated at the point, when the unconfined concrete reaches ultimate compression strain, for different cases is compared with the values determined based on the design equations from the code provisions including ACI 318 (2019), Eurocode 8 (1996), and SNI code (1997) as well as existing studies presented in Table 1. Through this comparison, it is possible to modify the proposed equations from the literature to include the effect of the beam reinforcement grade. The modified expression can then be used for calculating the nominal beam flexural strength with the HSS.

Fig. 15 shows the comparison of the effective slab width at the point, when the unconfined concrete reaches ultimate compression strain, among the current study, code provisions, and existing studies. All the cases considered in this study are plotted in Fig. 15. The code provisions generally have a lower effective slab width, and it means those code models underestimated the slab reinforcement contribution to the nominal beam flexural strength. The results obtained from the multi-truss approach show a similar higher  $B_{eff}$  as the studies in the literature, and it appeared that current model is able to capture the effect of the beam reinforcement grade.

The  $B_{eff}$  obtained from the multi-truss model is quite similar with those estimated from Zhen et al. (2009)

for the cases with the Grade 60 beam reinforcement, as shown in Fig. 15. Therefore, this study modifies the Zhen et al.'s equation to include the effect of the beam reinforcement grades. If Zhen et al.'s equation is taken as the  $B_{eff}$  for normal-strength steel ( $B_{eff,G60}$ ), a modification coefficient of  $\beta$  can be introduced, as follows:

$$B_{eff,G60} = b + 4h \text{ for Grade 60 } (f_y = 420 \text{ MPa}). \quad (5)$$

$$B_{eff} = \beta \times B_{eff,G60}. \quad (6)$$

$$\beta = \left( \frac{f_y}{420} \right)^{0.15}. \quad (7)$$

Fig. 16 shows a comparison of  $B_{eff}$  among the values calculated by using the proposed Eq. (6), Zhen et al.'s original equation, and simulation results from this paper. As presented in the Fig. 16, the proposed equation can reasonably capture the effect of the beam reinforcement grade on the slab effective width in a simple manner. In general, the proposed equation shows a slightly wider  $B_{eff}$  than the simulation results, which can be more conservative to satisfy the "strong column, weak beam" criterion.

### 6 Conclusions

This study investigates the slab contribution to the negative moment strength in the tension zone for T-beam configured with HSS in the exterior beam-column joints. The nonlinear pushover analyses were conducted on a multi-truss model of beam-column-slab assemblages to identify the effect of the beam reinforcement grade on the stress and strain distribution along the width of the slab. Moreover, the effects of other influential factors

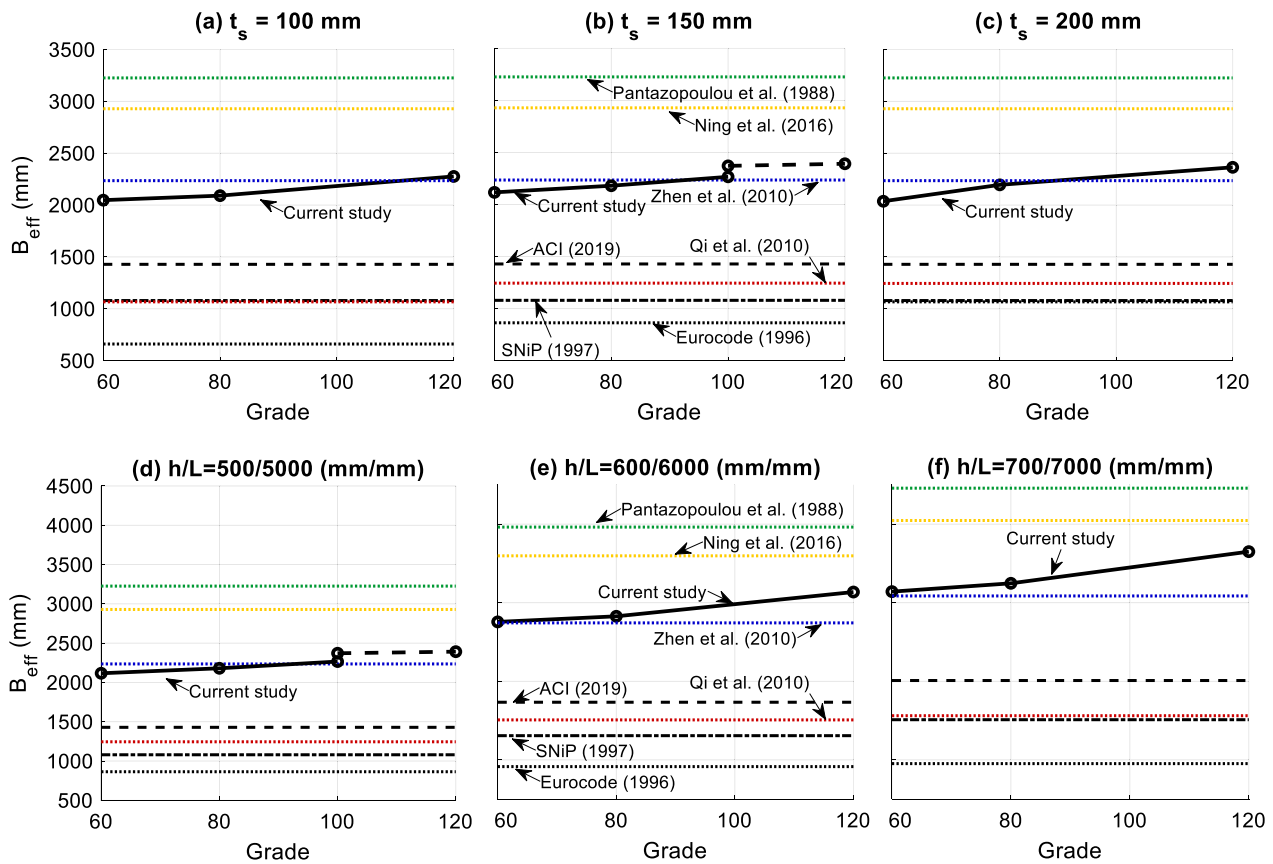


**Fig. 15** Comparison of the effective slab width at the concrete crushing point among this paper, code provisions, and existing studies

on the effective slab width were also considered, which includes the slab thickness, height, and span length of the beam. On this basis, the following conclusions can be drawn:

- The slab reinforcement can contribute to the beam flexural strength in the negative moment region. The contribution reduces as moving far from the center of the beam due to the shear lag effect, though.
- When the grade of the beam reinforcement increases, the behavior of beam-column-slab assemblage becomes more flexible under lateral loads. This higher flexibility results in a larger drift ratio at the point when the concrete in the beam reaches ultimate compression strain. The larger drift ratio at this point increases the stress/strain in the slab reinforcement, resulting in a wider effective slab width for the cases with HSS.
- The effective slab width increases with the increase of the drift ratio since the strain penetrates into more slab reinforcement. At large drift ratios, the effective slab width is insensitive to the beam reinforcement grade. However, at low drift ratios, this

width increases as the beam reinforcement grade increases, particularly at the point where the unconfined concrete reaches ultimate compression strain.

- The effective slab width for the negative moment is insensitive to the slab thickness since the concrete has cracked. On the other hand, the height/span length of the beam influences the effective slab width. However, its effect is independent of the one from the beam reinforcement grade.
- In general, design code provisions tend to have a lower effective slab width and underestimate the contribution of the slab reinforcement. The simulation results obtained from this paper as well as those from existing studies show a much higher effective slab width. The results from this paper indicate an effect of the beam reinforcement grade on the effective slab width.
- Based on the parametric study results, a modification coefficient was derived to incorporate the effect of the beam reinforcement grade on the effective slab width. This coefficient was applied to the design equation developed by Zhen et al. (2009) which shows a similar result for the case with normal-strength reinforcement.

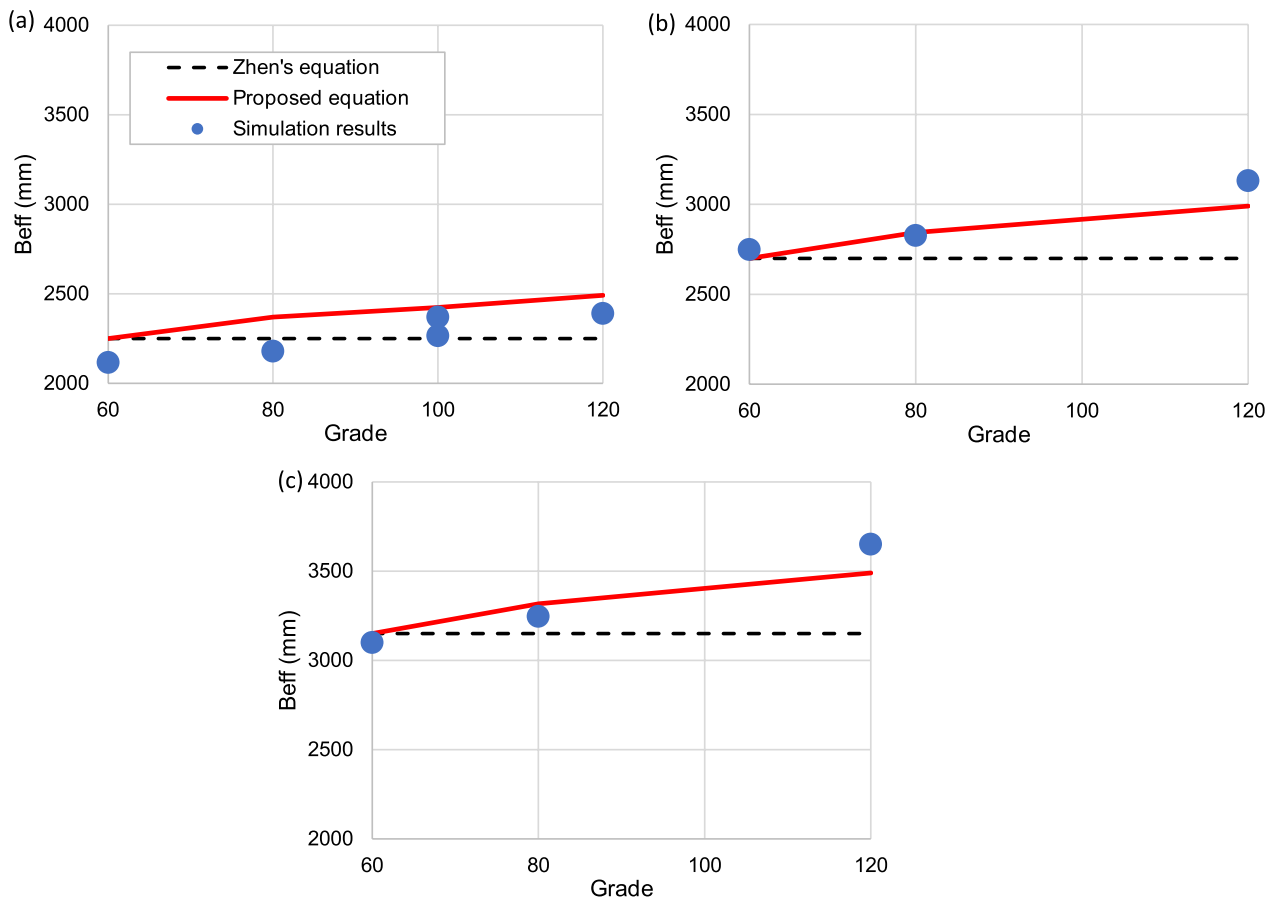


**Fig. 16** Effective slab width from the proposed equation: (a)  $h/L = 500/5000$  mm; (b)  $h/L = 600/6000$ ; (c)  $h/L = 700/7000$

- The proposed simple expression with the modification coefficient can reasonably capture the effective slab width obtained from the simulations, and it can be applied for the reinforced concrete T-beam configured with HSS in negative moment regions to estimate the beam nominal flexural strength with contributions of slab reinforcement.

This study was limited to the investigation of exterior beam-column joints. For the interior joint, the effective slab thickness might be different due to the effect of moment on the other side of the column. Therefore, this developed equation (Eq. 5) might only be applicable to the exterior beam-column joint and further validation is needed for the interior beam-column joint design. At the same time, the developed equation (Eq. 5) was purely from numerical simulations, and it might require validation from a further experimental study on the high-strength steel before applying it for the seismic design in the construction practices.

**Abbreviations**

$A$	Area of slab reinforcement
$A_D$	Area of diagonal truss element
$A_H$	Area of horizontal truss element
$b$	Longitudinal beam width
$b_c$	Column width
$B_{eff}$	Effective slab width
$B_{eff}'$	Overhanging effective slab width
$d$	Effective beam depth
$E_c$	Young's modulus of the concrete
$E_D$	Young's modulus of diagonal truss element
$E_H$	Young's modulus of horizontal truss element
$f'_c$	Compressive strength of concrete
$f_t$	Tensile strength of concrete
$F_{T,d}$	Tension forces assumed to be developed along the diagonal truss bar
$F_{C,d}$	Compression forces assumed to be developed along the diagonal truss bar
$F_{V,d}$	Vertical components of the forces along the diagonal truss
$F_y, \sigma_y$	Yield strength of reinforcement
$G_c$	Shear modulus of the concrete
$h$	Longitudinal beam height
$I_{long}$	Moment of inertia of the longitudinal beam
$I_{trans}$	Moment of inertia of the transverse beam
$K_{C/T}$	Total stiffness of the solid element
$K_{C/T,hor}$	Shear stiffness of horizontal element
$K_{C/T,diag}$	Shear stiffness of diagonal element
$L$	Beam span
$L_o$	Clear distance to the adjacent web

$L_D$	Length of diagonal truss element
$L_{D,v}$	Length of vertical component of elongated/shortened diagonal truss
$L_e$	Length of solid element
$L_H$	Length of horizontal truss element
$M_{nb}$	The nominal moment capacity of beams calculated at the surface of the joint
$M_{nc}$	The nominal moment capacity of columns calculated at the surface of the joint
$N$	Number of bars within the effective slab width
$s$	Slab reinforcement spacing
$t_s$	Slab thickness
$\beta$	Adjustment coefficient for $B_{eff}$ to include the effect of HSS
$\delta, \Delta$	Vertical displacement
$\nu$	Poisson's ratio of the concrete,
$\epsilon_{cu}$	Ultimate strain of concrete
$\epsilon_d$	Strain of diagonal truss element
$\theta$	Angle between horizontal and diagonal truss elements
$\rho$	Beam reinforcement ratio
$\sigma_C/T$	Tension/compression stress developing in solid element
$\sigma_j$	Stress in each slab reinforcement
$\tau$	Shear stress across the solid element surface

### Acknowledgements

Nazarbayev University funded this research under Faculty Development Competitive Research Grant No. 021220FD2151. The fourth author also would like to acknowledge the support from the National Research Foundation of Korea (KRF) grant funded by the Korea government (MSIT) (No. 2021R1C1C2093437). Any opinions, findings, conclusions, or recommendations expressed in this material are those of the author(s) and do not necessarily reflect the views of Nazarbayev University.

### Author contributions

ZM: formal analysis, investigation, visualization, writing—original draft. DS: data curation, investigation, validation. DZ: conceptualization, funding acquisition, investigation, methodology, supervision, writing—review and editing. HJ: funding acquisition, investigation, methodology, supervision, writing—review and editing. DL: conceptualization, methodology, resources, writing—review and editing. JK: funding acquisition, project administration, resources, supervision.

### Funding

Nazarbayev University: Research Grant No. 021220FD2151. National Research Foundation of Korea (KRF): 2021R1C1C2093437.

### Availability of data and materials

Not applicable.

### Declarations

#### Ethics approval and consent to participate

We confirm that we have given due consideration to the protection of intellectual property associated with this work and that there are no impediments to publication, including the timing of publication, with respect to intellectual property. In so doing we confirm that we have followed the regulations of our institutions concerning intellectual property.

#### Consent for publication

We confirm that the manuscript has been read and approved by all named authors and that there are no other persons who satisfied the criteria for authorship but are not listed. We further confirm that the order of authors listed in the manuscript has been approved by all of us.

#### Competing interests

Not applicable.

Received: 27 January 2023 Accepted: 14 August 2023

Published online: 22 December 2023

### References

- ABAQUS (2006) ABAQUS Analysis User's Manual (Version 6.6). Providence, RI: Dassault Systems SIMULIA Corporation.
- ACI Committee 318 (2019). *Building Code Requirements for Structural Concrete (ACI318-19) and Commentary*. Farmington Hills, MI: American Concrete Institute.
- Alaee, P., & Li, B. (2017). High-strength concrete exterior beam-column joints with high-yield strength steel reinforcements. *Engineering Structures*, *145*, 305–321.
- Alavi-Dehkordi, S., Mostofinejad, D., & Alaee, P. (2019). Effects of high-strength reinforcing bars and concrete on seismic behavior of RC beam-column joints. *Engineering Structures*, *183*, 702–719.
- Aoyama, H. (2001). *Design of modern highrise reinforced concrete structures* (Vol. 3). UK: Imperial College Press.
- ASTM (2016a). Standard specification for low-alloy steel deformed and plain bars for concrete reinforcement, ASTM A706-16, ASTM International, West Conshohocken, Pennsylvania.
- ASTM (2016b). Standard Specification for Deformed and Plain Carbon-Steel Bars for Concrete Reinforcement, ASTM A615-16, ASTM International, West Conshohocken, Pennsylvania.
- Barbosa, A. R., Link, T., & Trejo, D. (2016). Seismic performance of high-strength steel RC bridge columns. *Journal of Bridge Engineering*, *21*(2), 04015044.
- British Standards Institution. (1996). *Eurocode 8: Design provisions for earthquake resistance of structures*. British Standards Institution.
- Chang, B., Hutchinson, T., Wang, X., & Englekirk, R. (2014). Seismic performance of beam-column subassemblies with high-strength steel reinforcement. *ACI Structural Journal*, *111*(6), 1329–1338.
- Cheng, M. Y., Wibowo, L. S. B., Lequesne, R. D., & Lepage, A. (2016). Deformation capacity and strength of RC frame members with high-strength materials. *James K. Wight: A Tribute for his Students and Colleagues (ACI Special Publication SP-311)*, *311*, 6–1.
- Concrete Reinforcing Steel Institute (2016). *High-Strength Reinforcing Bars*. CRSI Technical Note ETN-M-8-16, Schaumburg, Illinois.
- Durrani, A. J., & Zerbe, H. E. (1987). Seismic resistance of R/C exterior connections with floor slab. *Journal of Structural Engineering*, *113*(8), 1850–1864.
- El-Hacha, R., & Rizkalla, S. H. (2002). *Fundamental material properties of MMFX steel rebars*. Research Report: RD-02/04, North Carolina State University.
- Huq, M. S. (2018). *HSS bars in earthquake-resistant T-shaped concrete walls*. [Doctoral dissertation, University of Kansas].
- Kotsovos, G. M., Vougioukas, E., & Kotsovos, M. D. (2013). Reducing steel congestion without violating seismic performance requirements. *Structural Journal*, *110*(3), 427–436.
- Li, Y., Cao, S., & Jing, D. (2018). Concrete columns reinforced with high-strength steel subjected to reversed cycle loading. *ACI Structural Journal*, *115*(4).
- Macias, J., Wright, M., Behr, O. G., & Valladares, V. (2017). Analysis of international standards on concrete reinforcing steel bar. *AISTech 2017 Proceedings*.
- Mamesh, Z. (2022). Investigation of slab reinforcement contribution to negative moment strength of reinforced concrete T-beam with high strength steel. Master Thesis, Nazarbayev University, Astana, Kazakhstan.
- Moffatt, K. R., & Dowling, P. J. (1978). British shear lag rules for composite girders. *Journal of the Structural Division*, *104*(7), 1123–1130.
- National Building Codes of Russia. (1997). SNIIP 2.03.01-84 Concrete and Reinforced Concrete Structures. Printed in USA.
- Ning, N., Qu, W., & Ma, Z. J. (2016). Design recommendations for achieving "strong column-weak beam" in RC frames. *Engineering Structures*, *126*, 343–352.
- NIST GCR 14-917-30 (2014). *Use of high-strength reinforcement in earthquake-resistant concrete structures*. NEHRP Consultants Joint Venture, National Institute of Standards and Technology, U.S. Department of Commerce.
- Panagiotou, M., Restrepo, J. I., Schoettler, M., & Kim, G. (2012). Nonlinear Cyclic Truss Model for Reinforced Concrete Walls. *ACI Structural Journal*, *109*(2).
- Pantazopoulou, S. J., Moehle, J. P., & Shahrooz, B. M. (1988). Simple analytical model for T-beams in flexure. *Journal of Structural Engineering*, *114*(7), 1507–1523.
- Qi, C. H., Li, S., Sun, Y., et al. (2010). Effect of floor slabs on the mechanical properties of reinforced concrete frame structures. *Journal of Catastrophology*, *25*(S0), 105–110.
- Shahrooz, B. M., Miller R.A., Harries K.A., & Russel H.G. (2011). *Design of concrete structures using HSS reinforcement* (Vol. 679). Transportation Research Board.

- Wang, M., Zhang, D., & Fu, J. (2016). Experimental evaluation of seismic response for reinforced concrete beam–column knee joints with irregular geometries. *Advances in Structural Engineering*, 19(12), 1889–1901.
- Zhen, S. J., Jiang, L. X., Zhang, W. P., et al. (2009). Experimental research and analysis of effective flange width of beam end section in cast-in-site concrete frames. *Structural Engineers*, 25(2), 134–140.
- Zhang, D., Fleischman, R. B., Naito, C. J., & Ren, R. (2011). Experimental evaluation of pretopped precast diaphragm critical flexure joint under seismic demands. *Journal of Structural Engineering*, 137(10), 1063–1074.
- Zhang, D., Fleischman, R., Naito, C. J., & Zhang, Z. (2016). Development of diaphragm connector elements for three-dimensional nonlinear dynamic analysis of precast concrete structures. *Advances in Structural Engineering*, 19(2), 187–202.

### Publisher's Note

Springer Nature remains neutral with regard to jurisdictional claims in published maps and institutional affiliations.

**Zhamilya Mamesh** Master Student, Nazarbayev University, 53 Kabanbay Batyr Ave, Astana, Republic of Kazakhstan, 010000.

**Dilnura Sailauova** Master Student, Nazarbayev University, 53 Kabanbay Batyr Ave, Astana, Republic of Kazakhstan, 010000.

**Dichuan Zhang** Associate Professor, Nazarbayev University, 53 Kabanbay Batyr Ave, Astana, Republic of Kazakhstan, 010000.

**Hyunjin Ju** is a Assistant Professor, Hankyong National University, 327, Jungang-ro, Anseong-si, Gyeonggi-do, 17579, Korea.

**Deuckhang Lee** is a Associate Professor, Chungbuk National University, 1 Chungdae-ro, Seowon-gu, Cheongju, Chungbuk 28644, Korea.

**Jong Kim** is a Professor, Nazarbayev University, 53 Kabanbay Batyr Ave, Astana, Republic of Kazakhstan, 010000.

Submit your manuscript to a SpringerOpen<sup>®</sup> journal and benefit from:

- ▶ Convenient online submission
- ▶ Rigorous peer review
- ▶ Open access: articles freely available online
- ▶ High visibility within the field
- ▶ Retaining the copyright to your article

---

Submit your next manuscript at ▶ [springeropen.com](https://www.springeropen.com)

---